Published in final edited form as:
J Neurosurg Pediatr. 2008 July ; 2(1): 75–82. doi:10.3171/PED/2008/2/7/075.

Quantitative diffusion tensor imaging and intellectual outcomes in spina bifida:

Laboratory investigation

Khader M. Hasan, Ph.D.[1], **Ambika Sankar, M.Sc.**[1], **Christopher Halphen, B.A.**[1], **Larry A. Kramer, M.D.**[1], **Linda Ewing-Cobbs, Ph.D.**[2], **Maureen Dennis, Ph.D.**[3], and **Jack M. Fletcher, Ph.D.**[4]

[1]Department of Diagnostic and Interventional Imaging, University of Texas Health Science Center at Houston

[2]Pediatrics University of Texas Health Science Center at Houston

[3]Hospital for Sick Children, Toronto, Ontario, Canada

[4]Department of Psychology, University of Houston, Texas

Abstract

Object—Patients with spina bifida (SB) have variable intellectual outcomes. The authors used diffusion tensor (DT) imaging to quantify whole-brain volumes of gray matter, white matter, and cerebrospinal fluid (CSF), and perform regional quantitative microstructural assessments of gray matter nuclei and white matter tracts in relation to intellectual outcomes in patients with SB.

Methods—Twenty-nine children with myelomeningoceles and 20 age- and sex-matched children with normal neural tube development underwent MR imaging with DT image acquisition and assessments of intelligence. The DT imaging-derived metrics were the fractional anisotropy (FA), axial (parallel), and transverse (perpendicular) diffusivities. These metrics were also used to segment the brain into white matter, gray matter, and CSF. A region-of-interest analysis was conducted of the white and gray matter structures implicated in hydrocephalus.

Results—The amount of whole-brain gray matter was decreased in patients with SB, with a corresponding increase in CSF ($p < 0.0001$). Regional transverse diffusivity in the caudate nucleus was decreased ($p < 0.0001$), and the corresponding FA was increased ($p < 0.0001$), suggesting reduced dendritic branching and connectivity. Fractional anisotropy in the posterior limb of the internal capsule increased in the myelomeningocele group ($p = 0.02$), suggesting elimination of some divergent fascicles; in contrast, the FA in several white matter structures (such as the corpus callosum genu [$p < 0.001$] and arcuate fasciculus) was reduced, suggesting disruption of myelination. Diffusion tensor imaging-metrics involving gray matter volume and the caudate nucleus, but not other structures, predicted variations in IQ ($r = 0.37$-0.50; $p < 0.05$).

Conclusions—Diffusion tensor imaging-derived metrics provide noninvasive neuronal surrogate markers of the pathogenesis of SB and predict variations in general intellectual outcomes in children with this condition.

Address correspondence to: Jack M. Fletcher, Ph.D., Department of Psychology, University of Houston Texas Medical Center Annex, 2151 West Holcombe Boulevard, Suite 222, Houston, Texas 77204-5053. jackfletcher@uh.edu..

Keywords

caudate nucleus; diffusion tensor imaging; IQ; myelomeningocele; neurodevelopment; spina bifida

Spina bifida myelomeningocele is a common neurogenetic disorder that causes abnormal functioning of the brain and spinal cord but is only infrequently associated with mental retardation.[14,27] The neural reorganization that supports preservation of intelligence in patients with SB is poorly understood. This reorganization reflects congenital injury to the neural tube and secondary hydrocephalus that includes configurational dysmorphological characteristics (such as a beaked tectum due to posterior fossa compression),[5] macrostructural volume loss in the cerebellum and posterior cortex,[27] dysgenesis of the corpus callosum,[5,14,27] and regional enhancement (such as an enlarged massa inter-media).[5] Although structural malformations and decreases in brain volume are associated with worse outcomes across neurogenetic disorders, little is known about microstructural assessments of structures other than the corpus callosum in SB and whether such variations are associated with better or worse outcomes.

Intellectual outcomes are highly variable in patients with SB. The rate of mental retardation is relatively low, and the authors of many older studies have reported preservation of verbal intelligence with a much higher rate of impairment of nonverbal IQ.[22,64] Authors of more recent studies with larger, more diverse patient cohorts have not found this difference in verbal and nonverbal IQ impairment, but have continued to find relatively low rates of mental retardation.[27] A variety of factors have been associated with variations in IQ, including the level of the lesion, number of shunt revisions and infections, and environmental factors.[22,27,64] An obvious source of variation is the extent to which the brain is congenitally malformed and further damaged by hydrocephalus. In addition to older studies based on pneumoencephalography and cerebral CT,[22] more recent studies have used MR imaging quantitative volumetry methods to assess regional brain volumes. These have shown reductions in gray and white matter volumes with corresponding increases in CSF volume in posterior brain areas in patients with SB. The authors of these studies did not assess specific structures other than the corpus callosum, and were restricted to large subdivisions of the brain.[26-28] Total cerebral volumes were comparable between children with SB and those in the control group, but cerebellar volumes were significantly lower in the SB group, especially in children with upper level (thoracic and above) spinal lesions.[27] There were weak correlations between intellectual and motor performance outcomes with increased CSF in the posterior areas of the brain and in area measurements of the corpus callosum. Few studies have assessed ROIs or brain microstructure using newer MR imaging methods such as DT imaging.

There are 2 preliminary DT imaging studies in patients with SB.[41,69] Vachha and colleagues[69] reported that qualitative DT imaging fiber tracking assessments of the fornices and cingulate yielded abnormal results in most of their 13 patients, and that only those with abnormal fornices showed lower memory performance on cognitive assessments. The present study is a larger and extended account of our preliminary quantitative DT imaging report.[41] We used a novel application of optimized whole-brain DT imaging at a high SNR to quantify white matter, gray matter, and CSF volumes in children with SB and in a control group. Regional metrics involving FA and axial and transverse diffusivities were obtained using a landmark-driven methodology. The DT imaging global and regional measures were correlated with IQ scores. We hypothesized that DT imaging assessments would show global reductions in gray and white matter with increased CSF volume comparable to those obtained with traditional MR imaging volumetric methods. Region-of-interest measurements

would be consistent with reduced white matter development and would correlate with lower IQ scores, a general measure of outcome in patients with SB.

Methods

Study Participants

Twenty-nine children with SB (mean age [± standard error of the mean] 13.2 ± 2.9 years, range 8.7–18 years) born with myelomeningocele (verified on medical record review and neurosurgical operative reports) and who underwent shunt placement for hydrocephalus were compared with a control group of 20 children with typical spinal cord development (mean age 11.8 ± 2.9 years, range 8–16.7 years). The age difference between the groups was not statistically significant ($p > 0.1$). The SB cohort included 13 girls and 16 boys of mixed ethnicities; 21 of 29 children were right-handed. The control group included 8 girls and 12 boys; 16 of 20 children were right-handed. The groups did not differ by age ($p = 0.10$, 2-tailed t-test), sex ($p = 0.09$, chi-square test), or handedness ($p = 0.07$, chi-square test). All children were primarily English speakers and in stable medical condition at the time of assessment. Written informed consent was obtained from guardians and adolescents, and assent from the participating children, in accordance with the University of Texas Health Science Center at Houston regulations for the protection of human research subjects.

Although DT imaging results can be influenced by edema and inflammatory lesions, no participants had edema or focal inflammatory lesions in any of the regions reported in this study as confirmed by a board-certified radiologist (L.A.K.) who reviewed the anatomical and fluid-attenuated images obtained in all participants. Additional coding of the qualitative characteristics of the MR images for expected features of SB revealed that 27 of 29 patients showed the characteristic Chiari malformation Type II of the hindbrain and cerebellum. The 2 patients who did not show this malformation had sacral lesions. Shunts were placed on the right side in 25 patients and on the left in 4. Consistent with findings in previous studies,[27] no child had a normal corpus callosum, with 15 showing dysgenesis of either the rostrum, splenium/posterior body, or both; in the other 14 thinning of some of the corpus callosum structure was evident. No child had undergone > 8 shunt revisions, and most children (71%) had undergone ≤ 2 revisions. The rate of shunt infections was 23%, with most revisions due to obstruction. One patient had an actively treated seizure disorder, 2 had received previous treatment for seizures, and the others had no history of seizures. There were 9 patients with thoracic, 16 with lumbar, and 4 with sacral level spinal lesions. Altogether, this group was similar to the 268-patient cohort we reported on previously.[27]

Intelligence Testing

Intelligence was assessed at the time of imaging with the Stanford-Binet Intelligence Test-4[67] in the group with SB, and the WASI[70] in the control group. The children in the control group were recruited from another study in which the same imaging sequences were used; the 2 measures are probably highly correlated because the WASI and WISC-III strongly correlate ($r = 0.92$), and the Stanford–Binet-4 and WISC-III also strongly correlate ($r = 0.81$).[61] As expected, the average IQ score in the control group (mean [± standard error of the mean] 106.4 ± 15.6, range 83–126) was significantly higher (and less variable) than in the children with SB (mean 79.5 ± 13.7, range 47–108; $p < 0.0001$, Mann–Whitney test). There were no significant differences between verbal and nonverbal IQ ($p > 0.10$).

Imaging Methods

We acquired whole-brain data using a Philips 3.0-T Intera system with a SENSE parallel imaging head coil. The MR imaging protocol included conventional imaging (3D spoiled

gradient echo and 3D fast spin echo) in the coronal plane, phase-sensitive MR imaging in the sagittal and axial planes, and matching axial diffusion-encoded data.

Acquisition—The diffusion weighted data were acquired using a single-shot spin echo diffusion sensitized echo planar imaging sequence with the balanced Icosa21 encoding scheme that uses 21 uniformly-distributed encoding directions, a diffusion sensitization of b-factor 1000 seconds/mm^2, a TR of 6100 msec, and a TE of 84 msec. Echo planar imaging distortion artifacts were reduced by using a SENSE acceleration factor or k-space undersampling of R of 2.[35,36,39-41,54] The slice thickness was 3.0 mm with 44 axial slices covering the entire brain (foramen magnum to vertex), a square field of view of 240 × 240 mm^2, and an image matrix of 256 × 256. The number of non–diffusion weighted or b-factor, ~ 0 magnitude image averages was 8; in addition, each encoding was repeated twice and magnitude-averaged to enhance the SNR.[7,16,38-40,57] Thus, 50 DT images were acquired for each of the 44 axial sections to cover the entire brain. The total DT imaging acquisition time was ~ 7 minutes, and resulted in SNR-independent DT imaging-metric estimation. The entire MR imaging data acquisition scan time was kept < 30 minutes to accommodate children.[38]

Processing—Although the raw DT images were acquired with fat suppression, all images were semiautomatically stripped to remove nonparenchymal tissue. Diffusion weighted data were distortion–corrected using the mutual information maximization approach.[54] The details of DT image processing are described elsewhere.[7,38-40]

Diffusion Tensor Imaging-Derived Metrics—Fractional anisotropy is a measure of the intravoxel directionality of water translational random motion in the presence of barriers and is expressed as a ratio ranging from 0 to 1 (0 = isotropic or no predilection for any particular direction, and 1 = unidirectional). Although the underlying histological processes leading to anisotropy changes in white matter detected on DT imaging are not completely understood,[8] factors that contribute to FA other than intravoxel orientation of the fibers include regional differences in fiber packing density, degree of myelination, fiber diameter, and density of the neuroglial cells. The mean diffusivity provides the overall magnitude of water diffusion (expressed in mm^{2}s^{-1}) and is a sensitive indicator of maturational changes in the brain independent of anisotropy measures. There are 2 specific diffusivity measures that can be derived from the DT data. The axial (parallel) ($\lambda_1 = \lambda_\parallel$) diffusivity is the magnitude of water movement along the long axis of axons, while the transverse (perpendicular) ($\lambda_t = \lambda_\perp$) diffusivity is the magnitude of water movement perpendicular to the long axis of the axons. The transverse diffusivity was defined as the mean of the minor (third) and medium (second) eigenvalues ($\lambda_\perp = (\lambda_2 + \lambda_3)/2$).[36] The axial and transverse diffusivities have been shown in animal models of human disease, and in DT imaging applications to human brain neurodevelopment and neurodegeneration to provide a more specific interpretation of DT imaging results than that provided by tensor anisotropy and mean diffusivity values.[8,34,35,40,65] Specifically, the axial diffusivity is more related to the intrinsic characteristics of the axons or changes in the extraaxonal/extracellular space, while the transverse diffusivity provides a more specific surrogate of changes associated with myelination.[8,40,53,65]

Tissue Segmentation—The collected DT imaging metrics and their corresponding errors were further used in a multidimensional, supervised, and trained feature space-initiated clustering procedure to segment the entire brain (cerebrum, brainstem, and cerebellum) into white matter, gray matter, and CSF. This new method uses the contrast in FA maps between CSF, white matter, and gray matter, and the cluster separability and discriminability of white matter and gray matter based on the principal diffusivity indices.[38] The CSF was segmented

based on its high diffusivity and low anisotropy.[38,57] Advantages of the DT imaging approach to multi-modal conventional MR imaging include: 1) the use of high SNR and uniformly distributed and rotationally invariant diffusion encoding scheme;[3,39,40] 2) the use of reduced image distortions with the adoption of parallel imaging;[42,65] 3) the utility of self-registered DT imaging metrics;[3,42] and 4) the fact that DT image processing involves decoupling of radio frequency inhomogeneity field-related intensity variations that are common in conventional MR imaging–based approaches.[35,58] The entire brain white matter, gray matter, and CSF fractions found using this approach are consistent with published reports using multispectral conventional MR imaging approaches in normative samples.[13,43,45,59] This is the first application of these DT imaging methods to a clinical sample.

Region-of-Interest Analysis—The ROI–derived from the analysis represented 50 "normal-appearing" white and gray matter structures, including the right–left (contralateral) cau-date head, putamen, internal capsule (anterior, external, and posterior limb), corpus callosum segments (Fig. 1),[38] corticospinal tract, forceps minor and major, inferior and superior longitudinal fasciculi, and the arcuate fasciculus and other gray matter regions (such as the cortex and hippocampus) and white matter structures (such as the cerebellar peduncles). The compact white matter structures belonged to 3 major categories: projection, commissural, and association fibers involved in inter- and intrahemispheric communication. The ROI placement procedure was supervised by a radiologist, and a 3D system was used that fused DT imaging maps with conventional MR images. This system has been shown to help reduce partial averaging artifacts due to CSF.[57] A subset of these ROIs was selected because of the expected impact from hydrocephalus and is reported here (Fig. 1).

Data Quality and Reproducibility—Water phantom measurements were collected over the span of the data acquisition to assure the field uniformity and stability of the MR unit. The diffusion encoding (Icosa21b) provided 3 levels of SNR, and thus the SNR dependence of the DT imaging–metrics reported in this work were also studied on all participants.[40] The ROI measurements were also examined for rater reproducibility.[39,41] All results were reproduced at multiple SNRs and rating sessions ($p > 0.9$).

Statistical Analysis

Group mean comparisons were made using the t-test for unpaired groups; within group comparisons were conducted using paired t-tests. Alpha levels were adjusted for the number of dependent univariate tests $M = 7$ ($p < 0.05/7 = 0.007$). Correlations with IQ were based on the Spearman correlation coefficient.

Results

In Fig. 2a the percentages (mean ± SD) of total white matter, gray matter, and CSF volume fractions in the groups are compared. Notice the significant increase in whole-brain CSF and significant decrease in whole brain gray matter percentages in the group with SB. The difference in white matter fraction was not statistically significant ($p > 0.8$). However, regional (mean ± SD) comparisons (Fig. 2b) of groups on the FA metric demonstrate that most white matter pathways are either not significantly different (anterior limb of internal capsule; $p > 0.5$) or show reduced FA (such as genu of the corpus callosum, arcuate fasciculus; $p < 0.02$), suggesting less integrity of these pathways because of reduced myelination or axonal packing. Consistent with this interpretation, the transverse water molecular diffusivity in the corpus callosum genu and association fibers (such as the arcuate fasciculus) was increased in patients with SB (Fig. 2c). In contrast, there is an increase in FA of the caudate nuclei in SB (Fig. 2c and d) due to an increase in the axial diffusivity and a more significant decrease in the transverse diffusivities. Other basal ganglia structures, such

as the putamen, did not show this pattern. There are also notable trends for decreased anisotropy of the arcuate fasciculus ($p \sim 0.02$) and increased FA in the posterior limb of the internal capsule ($p \sim 0.02$) that did not meet the critical level of alpha ($p < 0.007$). Altogether, these data show different changes in the white matter and gray matter nuclei of children with SB, suggesting different mechanisms affecting the brain after early injury.

Within the group with SB (29 patients), IQ significantly correlated with the total gray matter/total brain volume percentage ($r = 0.50$, $p = 0.005$) (Fig. 3 *left*). In addition, IQ significantly correlated regionally with the transverse diffusivity of the right caudate head ($r = 0.42$, $p = 0.024$) (Fig. 3 *right*) and left caudate head ($r = 0.37$, $p = 0.046$; data not shown). There were no significant correlations with other DT imaging measures.

Discussion

This is the first quantitative DT imaging-based report documenting patterns of global and regional white and gray matter volumes with assessments of brain microstructure and corresponding correlations with outcomes in children with SB. Our DT imaging measurements were conducted at high SNR using optimized DT imaging encoding schemes to minimize well-documented biases in DT imaging-metric estimation. Because CSF volume/brain volume fraction is significantly larger in the SB group, one would expect a reduction in FA due to contamination with CSF bordering the atrophic caudate (Fig. 1); on the contrary, we identified significant bilateral increases in caudate FA in the group with SB.

It is well-established that hydrocephalus in humans with SB[29,30] and in animals[11,33,60] disrupts the development of myelination and the overall development of the white matter, consistent with our observation of decreased FA in several pathways (such as the corpus callosum genu and arcuate). These changes may be partially reversed by early shunt placement,[18,19,33,72] which may lead to partial, but not complete, reconstruction of the cerebral mantle.[71] Decreased FA of the white matter has also been reported in disorders not associated with severe hydrocephalus, including Krabbe disease,[48] fragile X syndrome,[6] velocardiofacial syndrome,[62] and William syndrome[31] and is interpreted as a marker of reduced myelination. Elevated white matter FA, as observed in this study in the posterior limb of the internal capsule, may reflect greater alignment of fibers in the voxel as a result of elimination of divergent fibers,[2] developmental myelination,[52,53] remyelination,[48] or increased microfilament density in the axons as a result of training, adaptation, and functional specialization.[9]

In gray matter structures such as the caudate, increased FA and the commensurate increase in the axial diffusivity and reduction in the transverse diffusivity may be related to reduced dendritic branching.[41] Experimental models in animals have shown that infantile hydrocephalus leads to neuronal damage that is progressive and not completely reversed by shunt placement.[11,33,51,60] These changes affect neurotransmitter systems involved in learning[66] and in cortical and subcortical connectivity in afferent and nonafferent pathways.[25,44] There are also effects on dendritic formation that are only partially reversed by early shunt placement,[33,47] and in animal models are associated with impairments in learning, even after shunt insertion.[50]

Based on the results of DT imaging, Assaf et al.[2] reported that the compression of white matter as a result of acute hydrocephalus in humans reduces the FA of white matter structures, such as the genu of the corpus callosum. Assaf et al. also reported an increase in FA along with reduced trans-verse diffusivity in the posterior limb of internal capsule, hypothesizing elimination of some divergent fascicles traversing this region that subserves both sensory and motor functions. Our measurements of the posterior limb of the internal

capsule in older children with SB are consistent with these observations. Altogether, the effects of hydrocephalus on brain parenchyma have been well-studied in animals and humans, and include disruption of both neurons and axons, and causing cellular death, migrational defects, and other problems.[1,16,17] Our DT imaging measurements are sensitive to these changes and show continued effects of the early disruptive effects of hydrocephalus in these shunt-treated children.

Hydrocephalus has also been shown to affect the long-term potentiation of synaptic integration in experimental models.[68] As the increase in FA for the caudate is observed in children with SB who are well beyond the infantile period, these results may reflect prolonged disruption of the processes that underlie synaptic connectivity in the late postnatal period and continuing through adolescence.[43,45] Decreased dendritic arborization is the major mechanism underlying the reduction in gray matter volume that occurs in development and was recently interpreted as being responsible for individual differences in the relation of IQ and gray matter volumes in normal development.[13,46,59] In adult-onset Huntington disease, greater extent of anisotropy of the caudate has been related to a loss of dendritic connectivity[23] that also resulted in reduced caudate-thalamic-nigral and caudate–cortical connections resulting in loss of motor and cognitive function.[4] Our observation of elevated caudate anisotropy levels is unique to the pathogenesis of SB. For example, in fragile X syndrome, macrostructural volumes of the caudate were reported as larger than in controls, along with decreased diffusion anisotropy as a result of incoherent overproduction of dendrite connections that was negatively related to IQ.[6,31]

Results of recent DT imaging studies of the fetal cortex that included comparisons with histological studies also support the hypothesis of long-term effects on dendritic arborization in SB, indicating that gray matter anisotropy is largest at 26 weeks postgestation, and decreased to normal neonatal values as a result of dendrite formation.[24,32,49] In addition, DT imaging ROI studies of the basal ganglia of normal brain maturation and healthy aging indicate that the diffusion tensor anisotropy of the putamen,[12,63] caudate,[37] and lenticular nuclei[10] (combined putamen and globus pallidus) increases slowly with age, along with a steady decrease in caudate nuclei volume.[41] Although the histological causes of this increase in diffusion anisotropy have not yet been isolated, hypotheses related to dendritic elimination along with neuronal loss have been previously invoked to explain the loss of basal ganglia neurons and their complex network of fiber connections,[13,43] and are consistent with the negative effects of hydrocephalus on cortical development and dendritic branching.

An abnormal or “paradoxical” increase in caudate and putamen diffusion tensor anisotropy, along with a reduction in the mean diffusivity, has been reported in normal-appearing basal ganglia of patients with multiple sclerosis.[15] The authors ruled out gliosis, which would have resulted in more disorganization (such as reduced anisotropy and mean diffusivity), attributing this finding to axonal degeneration due to fiber transection in remote focal multiple sclerosis lesions. A significant increase in caudate anisotropy, along with a slight decrease in mean diffusivity, has also been reported in benign intracranial hypertension, which rules out cerebral edema as an explanation.[55]

The present study includes a relatively small number of patients that prevents analysis of relevant treatment factors (such as shunt placement) and we lack histological analyses using CSF metabolite analysis and postmortem data that would directly address the DT imaging–derived hypotheses about neuropathology.[19,56] However, our results are consistent with studies of CSF in humans and in animal model studies of hydrocephalus, which itself results in tissue displacement, disruption, demyelination, and elimination of certain pathways.[17,19,56] In the absence of comparisons with other origins of congenital hydrocephalus (such

as aqueductal stenosis, which is even more rare than SB, and a cohort for which we did not sample), we cannot show that these findings are specific to SB or that they reflect more than the effects of hydrocephalus. The lack of significant findings involving white matter volumes is surprising since MR imaging morphometry studies have reported reductions in both gray and white matter in children with early hydrocephalus.[26-28] However, the older MR imaging morphometry studies are not whole-brain analyses, with measurements of only the cortex. Finally, the cognitive assessments were restricted to IQ measures, which are a general proxy for overall outcomes, and not specifically related to the ROIs. Using MR imaging–based volumetry in children with SB, we have shown the relationship of variations in timing functions and cerebellar volumes, and focused attention with thinning of the posterior parietal region.[20,21] Future studies should test hypotheses about specific cognitive and motor functions and DT imaging measurements in addition to factors such as shunt and revision status.

Conclusions

Diffusion tensor-derived metrics such as total-brain gray matter percentage and regional FA and transverse diffusivity in the caudate provide important noninvasive neuronal surrogate markers of the pathogenesis of SB, and can be used to predict variations in cognitive outcomes associated with this condition. Mechanisms of neural reorganization in SB thus may include disruption of myelination, reduced dendritic branching, reduced connectivity, and the targeted elimination of some fiber types. Diffusion tensor imaging provides noninvasive markers of brain development and disruption in neurodevelopmental disorders that may ultimately assist in the investigation of the effects of shunt placement and other interventions in patients with neurodevelopmental disorders.

Acknowledgments

We thank Vipul Kumar Patel for helping in data acquisition.

This work was funded by NIH-NICHD grants P01-HD35946 awarded to Dr. Fletcher, and grant NICHD-R01-NS046308 awarded to Dr. Ewing-Cobbs. Additional funding to Dr. Hasan is provided by NINDS R01-NS052505-02.

Abbreviations used in this paper

CSF	cerebrospinal fluid
DT	diffusion tensor
FA	fractional anisotropy
ROI	region of interest
SB	spina bifida
SD	standard deviation
SNR	signal-to-noise ratio
WASI	Wechsler Abbreviated Scale of Intelligence
WISC	Wechsler Intelligence Scale for Children

References

1. Aoyama Y, Kinoshita Y, Yokota A, Hamada T. Neuronal damage in hydrocephalus and its restoration by shunt insertion in experimental hydrocephalus: a study involving the neurofilament-immunostaining method. J Neurosurg 2006;104(5 Suppl):332–339. [PubMed: 16848091]

2. Assaf Y, Ben-Sira L, Constantini S, Chang LC, Beni-Adani L. Diffusion tensor imaging in hydrocephalus: initial experience. AJNR Am J Neuroradiol 2006;27:1717–1724. [PubMed: 16971621]
3. Bammer R, Auer M, Keeling SL, Augustin M, Stables LA, Prokesch RW, et al. Diffusion tensor imaging using single-shot SENSE-EPI. Magn Reson Med 2002;48:128–136. [PubMed: 12111940]
4. Baquet ZC, Gorski JA, Jones KR. Early striatal dendrite deficits followed by neuron loss with advanced age in the absence of anterograde cortical brain-derived neurotrophic factor. J Neurosci 2004;24:4250–4258. [PubMed: 15115821]
5. Barkovich, AJ. Pediatric Neuroimaging. ed 4. Lippincott Williams & Wilkins; New York: 2005.
6. Barnea-Goraly N, Eliez S, Hedeus M, Menon V, White CD, Moseley M, et al. White matter tract alterations in fragile X syndrome: preliminary evidence from diffusion tensor imaging. Am J Med Genet B Neurosychiatr Genet 2003;118:81–88.
7. Basser PJ, Mattiello J, LeBihan D. Estimation of the effective self-diffusion tensor from the NMR spin echo. J Mag Reson B 1994;103:247–254.
8. Beaulieu C. The basis of anisotropic water diffusion in the nervous system—a technical review. NMR Biomed 2002;15:435–455. [PubMed: 12489094]
9. Bengtsson SL, Nagy Z, Skare S, Forsman L, Forssberg H, Ullén F. Extensive piano practicing has regionally specific effects on white matter development. Nat Neurosci 2005;8:1148–1150. [PubMed: 16116456]
10. Bhagat YA, Beaulieu C. Diffusion anisotropy in subcortical white matter and cortical gray matter: changes with aging and the role of CSF-suppression. J Mag Reson Imag 2004;20:216–227.
11. Boillat CA, Jones HC, Kaiser GL, Harris NG. Ultrastructural changes in the deep cortical pyramidal cells of infant rats with inherited hydrocephalus and the effect of shunt treatment. Exp Neurol 1997;147:377–388. [PubMed: 9344562]
12. Càmara E, Bodammer N, Rodríguez-Fornells A, Tempelmann C. Age-related water diffusion changes in human brain: a voxel-based approach. Neuroimage 2007;34:1588–1599. [PubMed: 17188516]
13. Caviness VS Jr, Kennedy DN, Richelme C, Rademacher J, Filipek PA. The human brain age 7-11 years: a volumetric analysis based on magnetic resonance images. Cereb Cortex 1996;6:726–736. [PubMed: 8921207]
14. Charney, E. Neural tube defects: Spina bifida and meningomyelocele. In: Batshaw, M.; Perret, Y., editors. Children with Disabilities: A Medical Primer. ed 3. Paul H. Brookes; Baltimore: 1992. p. 471-488.
15. Ciccarelli O, Werring DJ, Wheeler-Kingshott CA, Barker GJ, Parker GJ, Thompson AJ, et al. Investigation of MS normal-appearing brain using diffusion tensor MRI with clinical correlations. Neurol 2001;56:926–933.
16. Conturo TE, McKinstry RC, Aronovitz JA, Neil JJ. Diffusion MRI: precision, accuracy and flow effects. NMR Biomed 1995;8:307–332. [PubMed: 8739269]
17. Del Bigio MR. Cellular damage and prevention in childhood hydrocephalus. Brain Pathol 2004;14:317–324. [PubMed: 15446588]
18. Del Bigio MR, Kanfer JN, Zhang YW. Myelination delay in the cerebral white matter of immature rats with kaolin-induced hydrocephalus is reversible. J Neuropathol Exp Neurol 1997;56:1053–1066. [PubMed: 9291946]
19. Del Bigio MR, Wilson MJ, Enno T. Chronic hydrocephalus in rats and humans: white matter loss and behavior changes. Ann Neurol 2003;53:337–346. [PubMed: 12601701]
20. Dennis M, Edelstein K, Copeland K, Frederick J, Francis DJ, Hetherington R, et al. Covert orienting to exogenous and endogenous cures in children with spina bifida. Neuropsychologia 2005;43:976–987. [PubMed: 15716168]
21. Dennis M, Edelstein K, Hetherington R, Copeland K, Frederick J, Blaser SE, et al. Neurobiology of perceptual and motor timing in children with spina bifida in relation to cerebellar volume. Brain 2004;127:1292–1301. [PubMed: 15069019]
22. Dennis M, Fitz CR, Netley CT, Sugar J, Harwood-Nash DC, Hendrick EB, et al. The intelligence of hydrocephalic children. Arch Neurol 1981;38:607–615. [PubMed: 6975094]

23. Douaud, G.; Poupon, C.; Cointepas, Y.; Mangin, JF.; Gaura, V.; Golestani, N., et al. Diffusion tensor imaging (DTI) in Huntington's disease patients: analyses of fractional anisotropy (FA) maps and apparent diffusion coefficient (ADC) maps; ISMRM Workshop on Methods for Quantitative Diffusion MRI of Human Brain; Lake Louise, Canada. Berkeley, CA: ISMRM; 2005. 2005 (Abstract)
24. Dubois J, Hertz-Pannier L, Dehaene-Lambertz G, Cointepas Y, Le Bihan D. Assessment of the early organization and maturation of infants' cerebral white matter fiber bundles: a feasibility study using quantitative diffusion tensor imaging and tractography. Neuroimage 2006;30:1121–1132. [PubMed: 16413790]
25. Eskandari R, McAllister JP II, Miller JM, Ding Y, Ham SD, Shearer DM, et al. Effects of hydrocephalus and ventriculoperitoneal shunt therapy on afferent and efferent connections in the feline sensorimotor cortex. J Neurosurg 2004;101(2 Suppl):196–210. [PubMed: 15835108]
26. Fletcher JM, Bohan TP, Brandt ME, Kramer LA, Brookshire BL, Thorstad K, et al. Morphometric evaluation of the hydrocephalic brain: relationships with cognitive abilities. Childs Nerv Syst 1996;12:192–199. [PubMed: 8739405]
27. Fletcher JM, Copeland K, Frederick JA, Blaser SE, Kramer LA, Northrup H, et al. Spinal lesion level in spina bifida: a source of neural and cognitive heterogeneity. J Neurosurg 2005;102(3 Suppl):268–279. [PubMed: 15881750]
28. Fletcher JM, McCauley SR, Brandt ME, Bohan TP, Kramer LA, Francis DJ, et al. Regional brain tissue composition in children with hydrocephalus. Arch Neurol 1996;53:549–557. [PubMed: 8660158]
29. Friede RL. A quantitative study of myelination in hydrocephalus. J Neuropath Exp Neurol 1962;21:645–648. [PubMed: 13959738]
30. Gadsdon DR, Variend S, Emery JL. Myelination of the corpus callosum. II. The effect of relief of hydrocephalus upon the processes of myelination. Z Kinderchir 1979;25:314–321.
31. Gothelf D, Furfaro JA, Penniman LC, Glover GH, Reiss AL. The contribution of novel brain imaging techniques to understanding the neurobiology of mental retardation and developmental disabilities. Ment Retard Dev Dis Res Rev 2005;11:331–339.
32. Gupta RK, Hasan KM, Trivedi A, Pradhan M, Das V, Parikh NA, et al. Diffusion tensor imaging of the developing human cerebrum. J Neurosci Res 2005;81:172–178. [PubMed: 15931676]
33. Harris NG, McAllister JP II, Conaughty JM, Jones HC. The effect of inherited hydrocephalus and shunt treatment on cortical-pyramidal cell dendrites in the infant H-Tx rat. Exp Neurol 1996;141:269–279. [PubMed: 8812160]
34. Harsan LA, Poulet P, Guignard B, Steibel J, Parizel N, de Sousa PL, et al. Brain dysmyelination and recovery assessment by noninvasive in vivo diffusion tensor magnetic resonance imaging. J Neurosci Res 2006;83:392–402. [PubMed: 16397901]
35. Hasan KM. Diffusion tensor eigenvalues or both mean diffusivity and fractional anisotropy are required in quantitative clinical diffusion tensor MR reports: fractional anisotropy alone is not sufficient. Radiology 2006;239:611–613. Letter. [PubMed: 16641362]
36. Hasan KM. A framework for quality control and parameter optimization in diffusion tensor imaging: theoretical analysis and validation. Magn Reson Imaging 2007;25:1196–1202. [PubMed: 17442523]
37. Hasan KM, Halphen C, Boska MD, Narayana PA. Diffusion tensor metrics, T(2) relaxation, and volumetry of the naturally aging human caudate nuclei in healthy young and middle-aged adults: possible implications for the neurobiology of human brain aging and disease. Magn Reson Med 2008;59:7–13. [PubMed: 18050345]
38. Hasan KM, Halphen C, Sankar A, Eluvathingal T, Kramer LA, Stuebing KK, et al. Diffusion tensor imaging based tissue segmentation: Validation and application to the developing child and adolescent brain. Neuroimage 2007;34:1497–1505. [PubMed: 17166746]
39. Hasan KM, Narayana PA. Computation of the fractional anisotropy and mean diffusivity maps without tensor decoding and diagonalization: theoretical analysis and validation. Magn Reson Med 2003;50:589–598. [PubMed: 12939767]
40. Hasan KM, Narayana PA. Retrospective measurement of the diffusion tensor eigenvalues from diffusion anisotropy and mean diffusivity in DTI. Mag Reson Med 2006;56:130–137.

41. Hasan, KM.; Sankar, A.; Kramer, LA.; Ewing-Cobbs, L.; Brandt, ME.; Hannay, HJ., et al. Diffusion tensor imaging of spina bifida meningomylocele at 3.0T: preliminary evidence of neurodevelopmental brain plasticity; International Society of Magnetic Resonance in Medicine, 14th Meeting in Seattle; Washington. May 6–12, 2006; Berkeley, CA: ISMRM; p. 276Abstract
42. Jaermann T, Crelier G, Pruessmann KP, Golay X, Netsch T, van Muiswinkel AM, et al. SENSE-DTI at 3 T. Magn Reson Med 2004;51:230–236. [PubMed: 14755645]
43. Jernigan TL, Archibald SL, Berhow MT, Sowell ER, Foster DS, Hesselink JR. Cerebral structure on MRI, Part I: Localization of age-related changes. Biol Psychiat 1991;29:55–67. [PubMed: 2001446]
44. Kriebel RM, McAllister JP II. Pathology of the hippocampus in experimental feline infantile hydrocephalus. Neurol Res 2000;22:29–36. [PubMed: 10672578]
45. Lenroot RK, Giedd JN. Brain development in children and adolescents: insights from anatomical magnetic resonance imaging. Neurosci Biobehav Rev 2006;30:718–729. [PubMed: 16887188]
46. Masliah E, Mallory M, Hansen L, DeTeresa R, Terry RD. Quantitative synaptic alterations in the human neocortex during normal aging. Neurol 1993;43:192–197.
47. McAllister JP II, Maugans TA, Shah MV, Truex RC Jr. Neuronal effects of experimentally induced hydrocephalus in newborn rats. J Neurosurg 1985;63:776–783. [PubMed: 4056881]
48. McGraw P, Liang L, Escolar M, Mukundan S, Kurtzberg J, Provenzale JM. Krabbe disease treated with hematopoietic stem cell transplantation: serial assessment of anisotropy measurements-initial experience. Radiology 2005;236:221–230. [PubMed: 15987975]
49. McKinstry RC, Mathur A, Miller JH, Ozcan A, Snyder AZ, Schefft GL, et al. Radial organization of developing preterm human cerebral cortex revealed by non-invasive water diffusion anisotropy MRI. Cereb Cortex 2006;12:1237–1243. [PubMed: 12427675]
50. Miyazawa T, Sato K. Learning disability and impairment of synaptogenesis in HTX-rats with arrested shunt-dependent hydrocephalus. Childs Nerv Syst 1991;7:121–128. [PubMed: 1878865]
51. Mori F, Tanji K, Yoshida Y, Wakabayashi K. Thalamic retrograde degeneration in the congenitally hydrocephalic rat is attributable to apoptotic cell death. Neuropathology 2002;22:186–193. [PubMed: 12416558]
52. Mukherjee P, Miller JH, Shimony JS, Conturo TE, Lee BC, Almli CR, et al. Normal brain maturation during childhood: developmental trends characterized with diffusion-tensor MR imaging. Radiology 2002;221:349–358. [PubMed: 11687675]
53. Mukherjee P, Miller JH, Shimony JS, Philip JV, Nehra D, Snyder AZ, et al. Diffusion-tensor MR imaging of gray and white matter development during normal human brain maturation. AJNR Am J Neuroradiol 2002;23:1445–1456. [PubMed: 12372731]
54. Netsch T, van Muiswinkel A. Quantitative evaluation of image-based distortion correction in diffusion tensor imaging. IEEE Trans Med Imaging 2004;23:789–798. [PubMed: 15250631]
55. Owler BK, Higgins JN, Péna A, Carpenter TA, Pickard JD. Diffusion tensor imaging of benign intracranial hypertension: absence of cerebral oedema. Br J Neurosurg 2006;20:79–81. [PubMed: 16753621]
56. Pal K, Sharma U, Gupta DK, Pratap A, Jagannathan NR. Metabolite profile of cerebrospinal fluid in patients with spina bifida: a proton magnetic resonance spectroscopy study. Spine 2005;30:E68–E72. [PubMed: 15681999]
57. Pierpaoli C, Jezzard P, Basser PJ, Barnett A, Di Chiro G. Diffusion tensor MR imaging of the human brain. Radiology 1996;201:637–648. [PubMed: 8939209]
58. Rajapakse JC, DeCarli C, McLaughlin A, Giedd JN, Krain AL, Hamburger SD, et al. Cerebral magnetic resonance image segmentation using data fusion. J Comput Assist Tomogr 1996;20:206–218. [PubMed: 8606224]
59. Reiss AL, Abrams MT, Singer HS, Ross JL, Denckla MB. Brain development, gender and IQ in children. A volumetric imaging study. Brain 1996;119:1763–1774. [PubMed: 8931596]
60. Rubin RC, Hochwald GM, Tiell M, Mizutani H, Ghatak N. Hydrocephalus: I. Histological and ultrastructural changes in the pre-shunted cortical mantle. Surg Neurol 1976;5:109–114. [PubMed: 1257875]
61. Sattler, JM. Assessment of Children: Cognitive Applications. ed 4. Jerome M. Sattler; San Diego: 2001.

62. Simon TJ, Ding L, Bish JP, McDonald-McGinn DM, Zackai EH, Gee J. Volumetric, connective, and morphologic changes in the brains of children with chromosome 22q11.2 deletion syndrome: an integrative study. Neuroimage 2005;25:169–180. [PubMed: 15734353]

63. Snook L, Paulson LA, Roy D, Phillips L, Beaulieu C. Diffusion tensor imaging of neurodevelopment in children and young adults. Neuroimage 2005;26:1164–1173. [PubMed: 15961051]

64. Soare PL, Raimondi AJ. Intellectual and perceptual-motor characteristics of treated myelomeningocele children. Am J Disab Child 1977;131:199–204.

65. Song SK, Yoshino J, Le TQ, Lin SJ, Sun SW, Cross AH, et al. Demyelination increases radial diffusivity in corpus callosum of mouse brain. Neuroimage 2005;26:132–140. [PubMed: 15862213]

66. Tashiro Y, Drake JM. Reversibility of functionally injured neuro-transmitter systems with shunt placement in hydrocephalic rats: implications for intellectual impairment in hydrocephalus. J Neurosurg 1998;88:709–717. [PubMed: 9525718]

67. Thorndike, RL.; Hagen, EP.; Sattler, JM. The Stanford-Binet Intelligence Scale. ed 4. Riverside; Chicago: 1986.

68. Tsubokawa T, Katayama Y, Kawamata T. Impaired hippocampal plasticity in experimental chronic hydrocephalus. Brain Inj 1988;2:19–30. [PubMed: 2844349]

69. Vachha B, Adams RC, Rollins NK. Limbic tract anomalies in pediatric myelomeningocele and Chiari II malformation: anatomic correlations with memory and learning-initial investigation. Radiol 2006;240:194–202.

70. Wechsler, D. Wechsler Abbreviated Screening of Intelligence. Psychological Corporation; New York: 2001.

71. Yamada H, Yokota A, Furuta A, Horie A. Reconstitution of shunted mantle in experimental hydrocephalus. J Neurosurg 1992;76:856–862. [PubMed: 1564546]

72. Zhang YW, Del Bigio MR. Growth-associated protein-43 is increased in cerebrum of immature rats following induction of hydrocephalus. Neuroscience 1998;86:847–854. [PubMed: 9692721]

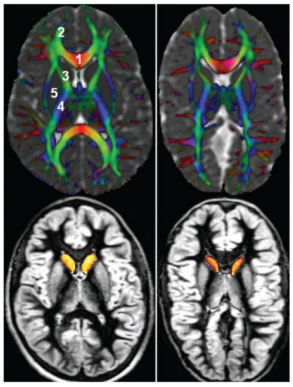

Fig. 1.

Representative images of the regions used for DT imaging quantification obtained in a child from the control group *(left)* and a child with SB *(right)*. The *upper panels* show a principal vector map modulated by FA and fused by the mean diffusivity to highlight CSF. Commissural (right-to-left) fibers appear *red*, association pathways *green*, and projection fibers *blue*. Cortical and deep gray matter appears gray in the upper panels and *bright gray* in the *lower panels*. The caudate nuclei are shown as *yellow/orange* in the *lower panels*. 1 = genu of the corpus callosum; 2 = minor forceps; 3 = anterior limb of the internal capsule; 4 = posterior limb of the internal capsule; 5 = putamen.

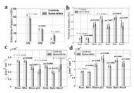

Fig. 2.

Bar graphs. a: Whole-brain DT imaging of gray matter (GM), white matter (WM), and CSF fractions (× 100%; means ± SDs) in the age-matched SB group (29 children) and control group (20 children). b: Region-of-interest DT imaging comparisons of FA in both groups. The ROIs selected include the right caudate head (Rcau), right putamen (RPut), right forceps minor (Rfmin), genu of the corpus callosum (gCC), right anterior and posterior limbs of the internal capsule (Ralic and Rplic, respectively), and the right arcuate fasciculus (RArcF). c: Region-of-interest DT imaging group comparisons of transverse diffusivities (λ_1) in both groups. d: Region-of-interest DT imaging group comparisons of axial diffusivities ($\lambda_\perp$) in both groups. The group means ± SDs are shown along with the corresponding probability values.

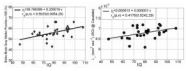

Fig. 3.

Spearman correlation coefficient and corresponding probability values of IQ with entire brain gray matter percentage derived using a DT imaging tissue segmentation approach *(left)*, and the regional transverse diffusivity in the cau-date nucleus head *(right)*.